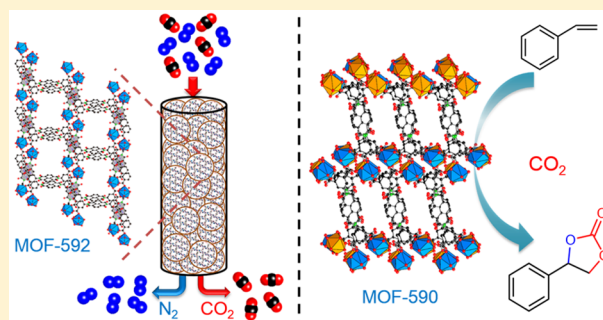


A Series of Metal–Organic Frameworks for Selective CO₂ Capture and Catalytic Oxidative Carboxylation of OlefinsHuong T. D. Nguyen,^{†,‡,§} Y. B. N. Tran,[‡] Hung N. Nguyen,[‡] Tranh C. Nguyen,[†] Felipe Gándara,^{*,§} and Phuong T. K. Nguyen^{*,†,‡,§}[†]Faculty of Chemistry, University of Science, Vietnam National University – Ho Chi Minh City, Ho Chi Minh City 721337, Vietnam[‡]Center for Innovative Materials and Architectures (INOMAR), Vietnam National University – Ho Chi Minh City (VNU-HCM), Ho Chi Minh City 721337, Vietnam[§]Departamento de Nuevas Arquitecturas en Química de Materiales, Materials Science Factory, Instituto de Ciencia de Materiales de Madrid (ICMM-CSIC), Sor Juana Inés de la Cruz 3, Cantoblanco 28049, Madrid, Spain

Supporting Information

ABSTRACT: Three new lanthanide-based metal–organic frameworks (Ln-MOFs), namely MOF-590, -591, and -592 constructed from a tetratopic linker, benzoimidephenanthroline tetracarboxylic acid (H₄BIPA-TC), were synthesized under solvothermal conditions and fully characterized. All of the new MOFs exhibit three-dimensional frameworks, which adopt unprecedented topologies in MOF field. Gas adsorption measurements of MOF-591 and -592 revealed good adsorption of CO₂ (low pressure, at room temperature) and moderate CO₂ selectivity over N₂ and CH₄. Consequently, breakthrough experiments illustrated the separation of CO₂ from binary mixture of CO₂ and N₂ with the use of MOF-592. Accordingly, MOF-592 revealed the selective CO₂ capture effectively without any loss in performance after three cycles. Moreover, MOF-590, -591, and -592 showed to be catalytically active in the oxidative carboxylation of styrene and CO₂ for a one-pot synthesis of styrene carbonate under mild conditions (1 atm CO₂, 80 °C, and without solvent). Among the new materials, MOF-590 revealed a remarkable efficiency with exceptional conversion (96%), selectivity (95%), and yield (91%).



INTRODUCTION

Metal–organic frameworks (MOFs) are crystalline materials that are formed by the linkage of inorganic and organic units via strong bonds resulting in porous structures.¹ Based on the principles of reticular chemistry, MOFs are designed by the appropriate choice of inorganic and organic building units, with well-defined geometrical features, to produce structures with targeted topologies.^{1,2} For those MOFs constructed from lanthanide-based inorganic clusters linked by multicarboxylic acid linkers, an extensive number of different three-dimensional (3D) networks have been reported.³ This is primarily due to the high variability in coordination environment of lanthanide cations. The use of Ln-based building units in the construction of new MOFs is attractive though because Ln cations typically have a high density of coordinated solvent ligands, which, when removed, can produce unsaturated metal sites that serve as gas binding or Lewis acidic sites.³ Moreover, hydroxyl ligands derived from water molecules binding to metal clusters have been exploited for their Lewis and/or Brønsted acidity in catalytic reactions.^{4,5} Therefore, lanthanide-based metal–organic frameworks (Ln-MOFs) are promising

candidates for the applications of gas capture^{6–9} and heterogeneous acid-catalyzed reactions.^{10–13}

The selective adsorption of CO₂ and subsequent transformation into fine chemicals is receiving great interest due to these application's environmental implications.^{14,15} Numerous studies have been devoted to the development of MOFs for reversible CO₂ adsorption based on the modification of their structural features and the presence of specific chemical functionalities.^{16–20} In this sense, the synthesis of cyclic carbonate from chemical fixation of CO₂ is an interesting approach to use CO₂ as an abundant and nontoxic chemical feedstock.²¹ There are extensive studies focused on the employment of new catalysts in the formation of cyclic carbonates from cycloaddition of CO₂.^{5,22–27} Furthermore, the direct synthesis of cyclic carbonate from olefins, so-called one-pot “oxidative carboxylation”, is an attractive and convenient approach because the transformation utilizes immediately the olefin without the requirement of isolating and purifying an epoxide substrate.²⁸ However, low catalytic efficiency in the

Received: August 13, 2018

Published: October 9, 2018

formation of cyclic carbonates and the appearance of side products obtained during the reaction limit its applicability, and only a few efficient catalytic systems and MOF catalysts have been exploited for this transformation up to now.^{22,29–31} Therefore, it is still necessary to develop heterogeneous catalysts suitable for the efficient synthesis of cyclic carbonates through the oxidative carboxylation reaction.

Herein, we report the synthesis and characterization of three new Ln-MOFs prepared with a tetratopic linker, benzoimide-phenanthroline tetracarboxylic acid ($H_4BIPA-TC$).³² This linker possesses a planar, π -acidic naphthalene core with diimide functionality, which favors π – π stacking interactions.³³ The resulting new MOFs, $[Nd_2(BIPA-TC)_{1.5}] \cdot 8H_2O$, $[Eu(H_2BIPA-TC)(BIPA-TC)_{0.5} \cdot 8H_2O][NH_2(CH_3)_2]$, and $[Tb(H_2BIPA-TC)(BIPA-TC)_{0.5} \cdot 6H_2O][NH_2(CH_3)_2]$ (denoted MOF-590, -591, and -592, respectively) exhibit 3D architectures with unprecedented topologies in MOF chemistry.³⁴ MOF-592 was proved effective as a potential candidate for the separation of CO_2 from a gas mixture of CO_2 and N_2 . In addition, MOF-590 was demonstrated to have remarkable catalytic activity on the oxidative carboxylation of styrene and CO_2 in the formation of styrene carbonate under mild conditions (0.18 mol % of MOF catalyst, 1 atm of CO_2 , 80 °C, 10 h), compared to other reported MOFs. Furthermore, MOF-590 was shown to be a robust catalyst and exhibited heterogeneous nature with no significant loss of catalytic performance over five consecutive cycles.

EXPERIMENTAL SECTION

Materials and General Procedures. The general procedures, starting materials, and synthesis of benzoimidephenanthroline tetracarboxylic acid ($H_4BIPA-TC$) linker can be found in the Supporting Information (SI), Sections S1 and S2. All chemicals for linker, MOF synthesis, and the catalytic reactions were purchased and used without purification. For comparison studies, commercial MOFs [HKUST-1 (Basolite C300), MOF-177 (Basolite Z377), ZIF-8 (Basolite Z1200), and Al-MIL-53 (Basolite A100)] were acquired and re-activated to obtain guest-free materials prior to conduct any measurement. Mg-MOF-74, UiO-67-bpydc, and Nd-BDC were prepared according to procedures previously reported (SI, Section S1).²²

Elemental microanalyses (EA) were performed using a LECO CHNS-932 Analyzer. Fourier transform infrared (FT-IR) spectra were obtained on a Bruker Vertex 70 with samples being well-dispersed in KBr pellets and the output signals are depicted as vs, very strong; s, strong; m, medium; sh, shoulder; w, weak; vw, very weak; or br, broad. Thermal gravimetric analysis (TGA) curves were measured on a TA Q500 thermal analysis system with the sample held in a platinum pan under a continuous flow of air. Low-pressure N_2 , CO_2 , and CH_4 adsorption isotherms were collected on a Micromeritics 3Flex with the use of He to estimate the dead space. A liquid N_2 bath was used for measurements at 77 K, and a circulating bath of ethylene glycol/water (1/1, v/v) was applied for measurements at 273, 283, and 298 K. Breakthrough measurements were performed using a L&C Science and Technology PSA-300-LC Analyzer with the bed column dimensions of 14×0.635 cm (l. \times i.d.). A ThermoStar GSD320 mass spectrometer was equipped with the system for monitoring of CO_2 , N_2 , H_2O , and O_2 from the gaseous effluent goes through the sample bed. Ultrahigh-purity grade N_2 , CH_4 , and He gases (99.999% purity) and high-purity grade CO_2 (99.995%) were used for all sorption experiments. 1H and ^{13}C nuclear magnetic resonance spectra (1H NMR, ^{13}C NMR) were recorded on a Bruker Advance II 500 MHz spectrometer. Gas chromatography (GC) analyses were performed on an Agilent GC System 19091s-433 equipped with a mass selective detector (Agilent 5973N) (GC-MS) using a capillary HP-5MS 5% phenyl methyl silox column (30 m \times 250 μm \times 0.25 μm) to

determine the products of the catalytic reaction. To determine the conversion, selectivity, and yield of catalytic reactions, GC analyses were carried out using an Agilent GC System 123–0132 equipped with a flame ionization detector (FID) and a capillary DB-1 ms column (30 m \times 320 μm \times 0.25 μm) with the use of biphenyl as an internal standard.

X-ray Diffraction Analysis. Single-crystal X-ray diffraction (SCXRD) analysis for MOF-590 and -592 was collected at 100 K on a Bruker four circle κ -diffractometer equipped with a Cu INCOATED microsource, operated at 30 W power (45 kV, 0.60 mA) to generate Cu $K\alpha$ radiation ($\lambda = 1.54178$ Å), with a Bruker VANTEC 500 area detector (MICROGAP technology). Single-crystal X-ray diffraction data for MOF-591 was performed on a Bruker D8 Venture diffractometer using monochromatic micro focus Cu $K\alpha$ ($\lambda = 1.54178$ Å) radiation source, operated at 50 W (50 kV, 1.0 mA) and equipped with a PHOTON 100 CMOS detector (100 K). The Bruker APEX3 program³⁵ was used for analysis of the raw data collection, and then SAINT³⁶ was applied for data reduction. An absorption correction was conducted using SADABS³⁷ routines. The crystal structures were solved by intrinsic phasing (SHELXT) and refined by full-matrix least-squares on F^2 (SHELXL-2014).³⁸ The solvent masking procedure in Olex2³⁹ program package was used to remove residual electron density from highly disordered solvent molecules, which were located in the pores of the structures. Powder XRD (PXRD) patterns were measured using a Bruker D8 Advance diffractometer with Ni-filtered Cu $K\alpha$ ($\lambda = 1.54178$ Å) radiation operated at 40 kV, 40 mA (1,600 W). The system was outfitted with an antiscattering shield to avoid incident diffuse radiation from hitting the detector. MOF samples were mounted on zero background holders and then well-flatted by a spatula. PXRD measurements were conducted with the 2θ range from 3 to 50°, a step size of 0.02°, and a fixed count time of 1 s per step.

Synthesis of MOF-590, $[Nd_2(BIPA-TC)_{1.5}] \cdot 8H_2O$. One mL of a solution of neodymium(III) nitrate hexahydrate (0.04 M, in H_2O) and 1 mL of a 0.04 M solution of $H_4BIPA-TC$ dissolved in dimethylacetamide (DMAc) were inserted into a Pyrex tube (o.d. \times i.d. = 10 mm \times 12 mm). This was followed by the addition of deionized water (4 mL) and glacial acetic acid (0.1 mL). Then, the tube was quickly sealed, sonicated for 30 min, and heated at 120 °C for 3 days to get yellow rectangular-shaped crystals. The as-synthesized MOF-590 crystals were then thoroughly washed with DMAc (3 \times 10 mL per day, for 3 days) and subsequently immersed in anhydrous ethanol (EtOH, 4 \times 10 mL per day, for 3 days). To obtain guest-free material, the ethanol-exchanged sample was evacuated under reduced pressure at room temperature for 18 h, followed by heating at 60 °C for an extra 24 h. E.A.: Calcd for $Nd_2C_{45}H_{31}N_3O_{26} = [Nd_2(BIPA-TC)_{1.5}] \cdot 8H_2O$: C, 41.00; H, 2.37; and N, 3.19%. Found: C, 41.26; H, 2.84; and N, 3.52%. FT-IR (KBr, 4000–400 cm^{-1}): 3430 (s, br), 1715 (s), 1678 (vs), 1620 (s), 1548 (s), 1451 (m), 1382 (m), 1349 (vs, sh), 1249 (s, sh), 1194 (w), 1119 (w).

Synthesis of MOF-591, $[Eu(H_2BIPA-TC)(BIPA-TC)_{0.5} \cdot 8H_2O][NH_2(CH_3)_2]$. 0.6 mL of a 0.043 M solution of europium(III) nitrate pentahydrate dissolved in deionized water and 15 mg of $H_4BIPA-TC$ (0.025 mmol) were placed in a 4 mL vial. This was followed by the addition of DMF (1 mL), deionized water (0.2 mL), and glacial acetic acid (0.25 mL). The vial was sealed and sonicated, then heated to 100 °C for 24 h to produce yellow rectangular-shaped crystals. The as-synthesized MOF-591 crystals were then thoroughly washed with DMF (3 \times 10 mL per day, for 3 days) and subsequently immersed in anhydrous EtOH (4 \times 10 mL per day for 3 days). To obtain the guest-free material, the ethanol-exchanged sample was evacuated under reduced pressure at room temperature for 18 h before heating at 50 °C for an additional 24 h. E.A.: Calcd for $EuC_{47}H_{41}N_4O_{26} = [Eu(H_2BIPA-TC)(BIPA-TC)_{0.5} \cdot 8H_2O][NH_2(CH_3)_2]$: C, 45.90; H, 3.36; and N, 4.56%. Found: C, 45.83; H, 3.39; and N, 4.44%. FT-IR (KBr, 4000–400 cm^{-1}): 3428 (s, br), 1713 (s), 1676 (vs), 1615 (s), 1577 (s), 1451 (m), 1389 (m), 1349 (vs, sh), 1295 (s, sh), 1196 (w), 1120 (w).

Synthesis of MOF-592, $[Tb(H_2BIPA-TC)(BIPA-TC)_{0.5} \cdot 6H_2O][NH_2(CH_3)_2]$. 0.6 mL of a 0.08 M solution of terbium(III) nitrate

hydrate dissolved in deionized water and 15 mg of $\text{H}_4\text{BIPA-TC}$ (0.025 mmol) were placed in a 4 mL vial. Following, DMF (1 mL), deionized water (0.2 mL), and glacial acetic acid (0.2 mL) were added to the vial. The vial was sealed and sonicated, then heated to 100 °C for 24 h to get yellow crystals with rectangular shape. The as-synthesized MOF-592 crystals were then thoroughly washed with DMF (3×10 mL per day, for 3 days) and subsequently immersed in anhydrous EtOH (4×10 mL per day, for 3 days). The ethanol-exchanged sample was evacuated under reduced pressure at room temperature for 18 h before heating at 50 °C for 24 h. E.A.: Calcd for $\text{TbC}_{47}\text{H}_{37}\text{N}_3\text{O}_{24} = [\text{Tb}(\text{H}_2\text{BIPA-TC})(\text{BIPA-TC})_{0.5} \cdot 6\text{H}_2\text{O}] \cdot [\text{NH}_2(\text{CH}_3)_2]$: C, 47.01; H, 3.11; and N, 4.67%. Found: C, 47.28; H, 3.21; and N, 4.60%. FT-IR (KBr, 4000–400 cm^{-1}): 3425 (s, br), 1712 (s), 1677 (vs), 1615 (s), 1578 (s), 1450 (m), 1384 (m), 1349 (vs, sh), 1252 (s, sh), 1199 (w), 1120 (w).

One-Pot Oxidative Carboxylation of Styrene and CO_2 . In a model experiment, the catalytic reaction was conducted using styrene (3.9 mmol), activated MOF catalyst (0.18 mol % ratio based on the molecular weight, $[\text{Nd}_2(\text{BIPA-TC})_{1.5} \cdot 8\text{H}_2\text{O}]$, $[\text{Eu}(\text{H}_2\text{BIPA-TC})(\text{BIPA-TC})_{0.5} \cdot 8\text{H}_2\text{O}][\text{NH}_2(\text{CH}_3)_2]$, $[\text{Tb}(\text{H}_2\text{BIPA-TC})(\text{BIPA-TC})_{0.5} \cdot 6\text{H}_2\text{O}][\text{NH}_2(\text{CH}_3)_2]$ for MOF-590, -591, and -592), anhydrous *tert*-butyl hydroperoxide (TBHP in decane, 7.4 mmol), and $n\text{Bu}_4\text{NBr}$ (0.31 mmol, 8 mol %) in a 25 mL Schlenk tube. The mixture reaction was evacuated thoroughly to remove gas impurities, then purged three times with CO_2 and kept at a constant pressure (~ 1 atm) with the use of a balloon filled with CO_2 . The reaction mixture was stirred at 80 °C for 10 h and monitored by analyzing with GC regularly taken aliquots. After completion of reaction, the mixture was cooled down in an ice bath, and the unreacted CO_2 was purged. The MOF catalyst was removed by centrifugation, and an aliquot of the reaction was analyzed by GC-FID using biphenyl as the internal standard to determine the catalytic conversion, selectivity, and yield of reaction. For the recycling experiment, the recovered catalyst was rinsed with ethyl acetate (3×3 mL) before heating at 50 °C under vacuum for 24 h and then reused for the next cycles.

RESULTS AND DISCUSSION

Crystal Structures of MOF-590 to -592. The ToposPro (v.5.3) software program⁴⁰ was employed to simplify the structures of MOF-590 to -592 and to classify the respective underlying net. The tetratopic linker was considered as two triangular nodes.⁴¹ The details of structural elucidation are provided in the SI, Section S4.

MOF-590. The single-crystal structure of MOF-590 was solved in the triclinic *P*-1 space group (no. 2) with lattice parameters $a = 10.260$ Å, $b = 12.999$ Å, $c = 19.851$ Å, $\alpha = 88.684(6)^\circ$, $\beta = 82.492(5)^\circ$, and $\gamma = 73.636(5)^\circ$ (Table 1). Its asymmetric unit contains two crystallographically independent Nd(III) ions, one and half BIPA-TC⁴⁻ ligands, and eight coordinated water molecules. In MOF-590's structure, the first Nd atom, Nd_1 , is bound to six carboxylate-O atoms from four BIPA-TC ligands and three additional water ligands. The corresponding simplified secondary building unit (SBU) adopts a tetrahedral geometry. The second Nd center, Nd_2 , forms a dimeric SBU, with two bridging and two chelating carboxylate groups. Five water ligands complete the coordination sphere of each one of the Nd atoms. The simplified SBU can be viewed as a parallelogram, with four points of extensions (Figure 1A). Interestingly, the overall framework topology of MOF-590 is a new net, denoted **nkp**, with a point symbol of $(4 \times 10^2)_2(4.6.8^4)_2(4.6^2)_2(4^2.6^2.8^2)(6^2.8)_2$ due to the linkage of two distinct types of 4-c inorganic SBUs and three distinct types of 3-c nodes upon simplifying the organic linkers (Figure 1B,C and SI, Section S4, Figure S7). According to PLATON calculations,⁴² MOF-590 has a $\sim 15.1\%$ void space in fully desolvated form, and the pore volume is $0.085 \text{ cm}^3 \text{ g}^{-1}$.

Table 1. Crystal Data and Structure Refinement for MOF-590, MOF-591, MOF-592

	MOF-590	MOF-591	MOF-592
empirical formula	$\text{C}_{45}\text{H}_{15}\text{N}_3\text{Nd}_2\text{O}_{26}$	$\text{C}_{47}\text{H}_{31}\text{EuN}_4\text{O}_{21}$	$\text{C}_{53}\text{H}_{28}\text{N}_6\text{O}_{22}\text{Tb}$
formula weight (g mol^{-1})	1302.08	1139.72	1259.73
crystal system	triclinic	triclinic	triclinic
space group	<i>P</i> -1	<i>P</i> -1	<i>P</i> -1
<i>a</i> (Å)	10.2605(9)	10.6709(12)	10.6566(3)
<i>b</i> (Å)	12.9996(15)	18.1669(19)	18.1300(5)
<i>c</i> (Å)	19.8518(17)	18.767(2)	19.5006(5)
α (deg)	88.684(6)	109.774(2)	65.601(2)
β (deg)	82.492(5)	102.201(2)	74.964(2)
γ (deg)	73.636(5)	97.897(2)	81.317(2)
<i>V</i> (Å ³)	2518.6(4)	3258.8(6)	3309.53(17)
<i>Z</i>	2	2	2
$\rho_{\text{calc}}(\text{g cm}^{-3})$	1.717	1.162	1.264
$\mu(\text{Cu K}\alpha)$ (mm^{-1})	16.365	7.446	5.874
R_{int}	0.1018	0.2496	0.1031
R_1^a	0.0603	0.0871	0.0566
wR_2^b	0.1575	0.2231	0.1585

^a $R_1 = \sum ||F_o| - |F_c|| / \sum |F_o|$. ^b $wR_2 = [\sum w(F_o^2 - F_c^2)^2 / \sum w(F_o^2)]^{1/2}$ for 3514 reflections satisfying $I > 2\sigma(I)$ (MOF-590), for 3428 reflections satisfying $I > 2\sigma(I)$ (MOF-591), for 8672 reflections satisfying $I > 2\sigma(I)$ (MOF-592).

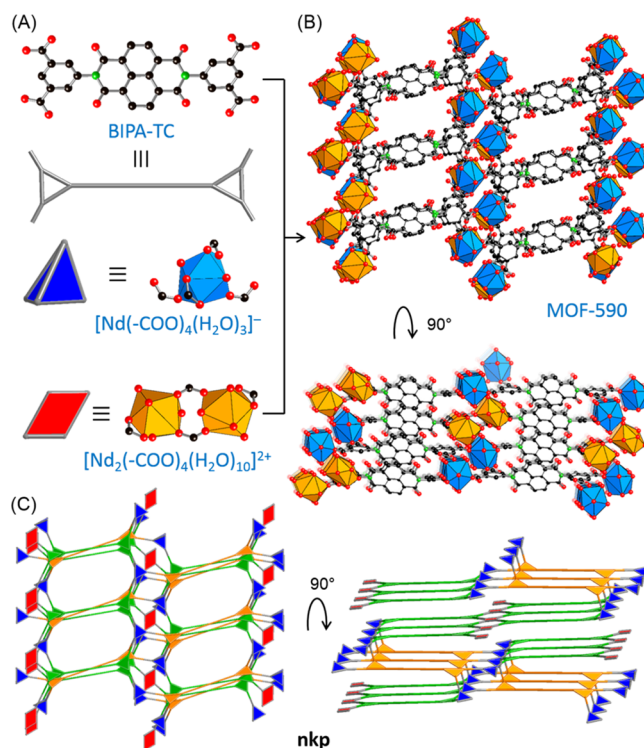


Figure 1. Single-crystal structure of MOF-590. (A) Connection of BIPA-TC and tetrahedral-shaped $[\text{Nd}(-\text{COO})_4(\text{H}_2\text{O})_3]^-$ and parallelogram-shaped $[\text{Nd}_2(-\text{COO})_4(\text{H}_2\text{O})_{10}]^{2+}$ SBUs result in (B) MOF-590. (C) The structure of MOF-590 exhibits the new **nkp** topology. Color scheme: Nd, blue and orange polyhedra; C, black; O, red; N, green; all H atoms are omitted for clarity.

MOF-591 and MOF-592. SCXRD analyses revealed that MOF-591 and -592 are isostructural frameworks, with identical

connections and conformations of Eu and Tb, respectively. We found that the diffracting quality of the MOF-591 crystals was lower than that of the MOF-592 (SI, Section S3). Thus, we describe here in detail the crystal structure of MOF-592 as a representative example. Accordingly, MOF-592 crystallizes in the triclinic *P*-1 space group (no. 2) with lattice parameters of $a = 10.657 \text{ \AA}$, $b = 18.130 \text{ \AA}$, $c = 19.501 \text{ \AA}$, $\alpha = 65.601(2)^\circ$, $\beta = 74.964(2)^\circ$, and $\gamma = 81.317(2)^\circ$ (Table 1). Its asymmetric unit contains one crystallographically independent Tb(III) ion, one partially deprotonated $\text{H}_2\text{BIPA-TC}^{2-}$ ligand, a half fully deprotonated BIPA-TC^{4-} ligand, one coordinated water molecule, two coordinated DMF molecules, one dimethylammonium (DMA^+) cation, and one water molecule. The Tb cluster in MOF-592 framework is found to be a dinuclear $[\text{Tb}_2(\text{COO})_8(\text{DMF})_4(\text{H}_2\text{O})_2]^{2-}$ SBU (Figure 2A). In partic-

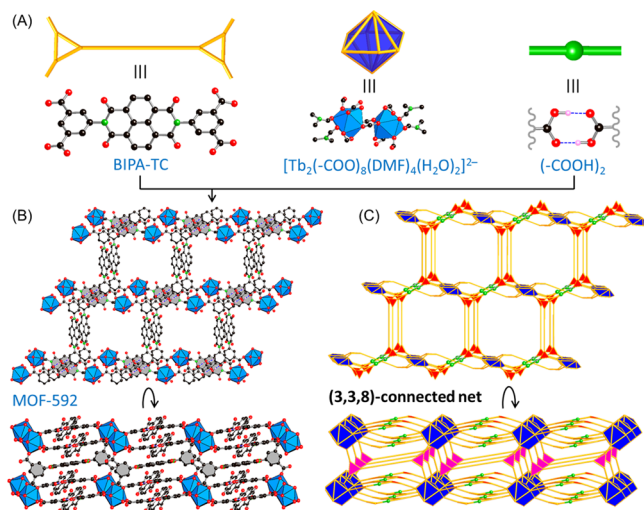


Figure 2. Single-crystal structure of MOF-592. (A) Connection of BIPA-TC and $[\text{Tb}_2(-\text{COO})_8(\text{DMF})_4(\text{H}_2\text{O})_2]^{2-}$ SBUs results in (B) MOF-592. (C) MOF-592 exhibits the new (3,3,8)-connected topology. Atom colors: Tb, blue polyhedra; C, black; O, red; N, green; H of protonated $-\text{COOH}$ group, pink spheres; all H atoms, except those involved in hydrogen bonding, are omitted for clarity.

ular, two carboxylate moieties coordinate in a bridging fashion to two Tb cations, two carboxylate functionalities connect in dimonodentate fashion, and four carboxylate groups are in monodentate type. Solvent molecules, including of DMF and water, complete the coordination spheres of the Tb atoms, and DMA^+ cations act as counterions occupying the pores. Interestingly, there are hydrogen bonds between the protonated carboxylate groups of the linkers, which construct a zigzag chain $(\text{H}_2\text{BIPA-TC})^{2-}_n$ that extends along the $[100]$ direction. Topological analysis reveals that the 3D framework of MOF-592 belongs to a new trinodal topology with a point symbol of $(4.6^2)_2(4^2.6^{12}.8^{14})(6^2.8)_4$ resulting from the linking

of 8-c inorganic SBUs and three different kinds of 3-c nodes derived from the organic linkers (Figure 2B,C, and SI, Section S4, Figure S8). According to PLATON,⁴² the void space of MOF-592 in its fully desolvated form is 47.6%, and the pore volume is $0.43 \text{ cm}^3 \text{ g}^{-1}$.

Structural Characterization, Including Porosity, and CO_2 Adsorption Properties. The synthesis of bulk MOF-590 to -592 was confirmed by PXRD analysis, whereas the diffraction patterns of as-synthesized samples were in agreement with those simulated from the single-crystal data (SI, Section S5, Figures S9–S11). The solvent-exchanged MOF-590 to -592 were activated under vacuum, first at room temperature for 16 h, and then heating at 50°C for 24 h. The PXRD profiles of the activated MOF-590 and -591 exhibited no appreciable changes compared with those of the corresponding as-synthesized samples, confirming that the structural integrity of MOF-590 and -591 was fully retained after activation (SI, Figures S9–S10). Otherwise, the PXRD pattern of activated MOF-592 showed broadened and slightly shifted peaks, suggesting a possible structural change attributed to the loss of guest solvent molecules (SI, Figure S11). In addition, chemical stability tests were also conducted on the Ln-MOFs, in which all activated Ln-MOF samples were immersed in water, acidic ($\text{pH} = 4.0$, aqueous acetic acid), and basic conditions (aqueous sodium hydroxide, $\text{pH} = 12$) at room temperature for 1 week. In the case of MOF-590, a loss of crystallinity was appreciated for the basic treated sample, while only differences in the high-angle area diffraction peaks were observed for the water and acid treated samples, as expected (SI, Figure S12). On the contrary, MOF-591 and -592 were noted to be unstable under the selected basic or acid conditions.

The thermal stability of MOF-590 to -592 was evaluated by recording the thermal gravimetric analysis (TGA) on the activated MOF-590 to -592 under airflow (SI, Section S6). Accordingly, the TGA curves exhibited no considerable weight loss up to 400°C , indicating the high thermal stability of these Ln-MOFs (SI, Figures S13 and S15). The significant weight loss observed at $\sim 400^\circ\text{C}$ in each TGA curve was associated with framework decomposition. The analyzed metal oxide residue weight percent for MOF-590 (27.6%), MOF-591 (15.2%), and MOF-592 (16.5%) was found to be in agreement with the corresponding calculated value according to elemental microanalysis (25.3, 14.3, and 15.2%, respectively).

The porosity of MOF-590 to -592 was assessed by performing the N_2 adsorption isotherms at 77 K. Accordingly, MOF-590 exhibited a nonporous behavior due to the restricted pore size and narrow pore volume natures. Otherwise, MOF-591 and -592 revealed Type-I isotherm, typical of microporous materials (SI, Figure S16). Furthermore, the isotherm of MOF-592 shows a small additional step with hysteresis around $P/P_0 = 0.05$, indicating framework flexibility or guest molecule

Table 2. Summary of the Surface Area, CO_2 Uptake Capacity, and CO_2/N_2 and CO_2/CH_4 Selectivities for MOF-591 and MOF-592

MOF	A_{BET} ($\text{m}^2 \text{ g}^{-1}$) ^a	CO_2 uptake ($\text{cm}^3 \text{ g}^{-1}$) ^b	N_2 uptake ($\text{cm}^3 \text{ g}^{-1}$) ^b	CH_4 uptake ($\text{cm}^3 \text{ g}^{-1}$) ^b	Q_{st} (kJ mol^{-1}) ^c	CO_2/N_2 selectivity ^d	CO_2/CH_4 selectivity ^d
MOF-591	960	36	2.3	7.4	23	21	5.6
MOF-592	900	42	2.1	7.0	22	27	6.8

^aCalculated by BET method. ^bAt 800 Torr and 298 K. ^cCalculated by virial-type expansion equation at near-zero CO_2 coverage. ^dCalculated from the ratios of the initial slope of pure component isotherms based on Henry's Law.

rearrangement. From these isotherm curves, the Brunauer–Emmett–Teller (BET)/Langmuir surface areas for MOF-590 to -592 were estimated to be 0, 960/1100, and 900/990 $\text{m}^2 \text{g}^{-1}$, respectively. These values were in good agreement with the theoretical accessible surface areas derived from crystal structure data of MOF-590, -591, and -592 (0, 1010, and 917 $\text{m}^2 \text{g}^{-1}$, respectively).

CO₂ Adsorption and Breakthrough Measurement.

Thermodynamic Uptake Capacity. To evaluate the gas adsorption properties, single component of CO₂, N₂, and CH₄ adsorption isotherms were performed at 273, 283, and 298 K for MOF-590 to -592 (SI, Section S6, Figures S17–22). As depicted in Table 2, MOF-592 displays the highest CO₂ capacity among the new materials, with an uptake of 42 $\text{cm}^3 \text{g}^{-1}$ at 800 Torr and 298 K. On the other hand, the N₂ and CH₄ uptake show low capacities (2.1 and 7.0 $\text{cm}^3 \text{g}^{-1}$, respectively) at identical temperature and pressure, which highlights the potential of this MOF for CO₂ capture and separation (Figure 3). Consequently, the coverage-dependent

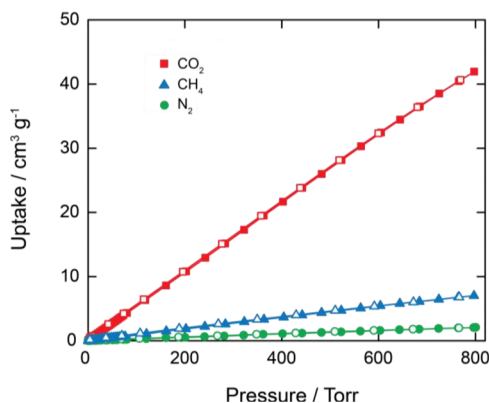


Figure 3. CO₂ (red), CH₄ (blue), and N₂ (green) isotherms at 298 K of MOF-592. Adsorption and desorption branches are marked by filled and open symbols, respectively. The connecting curves are guides for the eye.

isosteric enthalpy of adsorption (Q_{st}) for the studied gases (CO₂, N₂, and CH₄) were calculated using a virial-type expansion equation to fit the corresponding isotherms collected at 273, 283, and 298 K (SI, Figures S23). As shown in Table 2, the CO₂ adsorption enthalpies at near-zero coverage for MOF-591 and -592 were found to be relatively high, with values of 23 and 22 kJ mol^{-1} , respectively. To confirm the ability of selective CO₂ adsorption, the CO₂/N₂ and CO₂/CH₄ selectivities for MOF-591 and -592 were estimated from the ratios of the initial slope of pure component isotherms using Henry's law (Table 2 and SI, Section S6). Accordingly, MOF-592 revealed the highest selectivity toward CO₂ over N₂ and CH₄ (27 and 6.8, respectively). Subsequently, a dynamic breakthrough experiment was performed on MOF-592 with the binary mixture of CO₂ and N₂ to evaluate the reliability of those gas selectivity calculations and further demonstrate the CO₂ separation property.

Dynamic Adsorption Capacity via Breakthrough Measurement. A bed packed with MOF-592 was exposed to a 20 mL min^{-1} flow of a 16% dry mixture of CO₂ in N₂ at room temperature (SI, Section S7).¹⁸ As expected, only CO₂ was captured in the bed while N₂ passed through (Figure 4). This observation demonstrates that MOF-592 proceeds complete

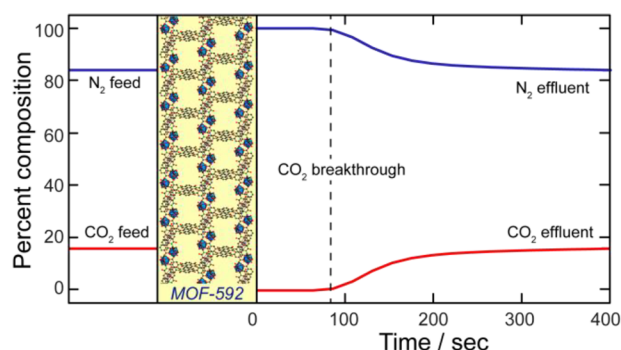


Figure 4. A binary mixture of CO₂/N₂ is flown through a fixed bed of MOF-592. The dashed line indicates the breakthrough time.

separation of CO₂ from the N₂ stream. From the breakthrough data, the dynamic CO₂ uptake capacity in the CO₂/N₂ separation was calculated to be 6.2 $\text{cm}^3 \text{g}^{-1}$ (1.2 wt %). To ensure the recyclability and facile regeneration of MOF-592, dynamic breakthrough measurements on activated MOF-592 were conducted over three cycles, without loss of performance (SI, Figures S24). Furthermore, MOF-592 could be fully regenerated by simply flowing pure N₂ through the MOF-loaded bed.

One-Pot Oxidative Carboxylation of Styrene and CO₂.

MOF-590 is built up from Nd clusters that have a large number of coordinated H₂O molecules (3 and 5 molecules per Nd₁ and Nd₂ center, respectively), which in principle can provide accessible catalytic Lewis and/or Brønsted sites. The resulting activated MOF-590 decorated with a high density of active acidic sites, along with presence of π -acidity derived from naphthalene diimide functionality of the H₄BIPA-TC linker, was proposed to effectively catalyze the oxidative carboxylation of styrene and CO₂. Since the size of styrene ($9.8 \times 7.1 \text{ \AA}^2$, optimized by Gaussian 09)⁴³ is larger than the pore aperture metrics of MOF-590 ($8.4 \times 2.5 \text{ \AA}^2$), the catalytic activity will only be due to the Nd³⁺ ions that exist on the external surface of MOF-590. The chemical and thermal stabilities of MOF-590 were previously demonstrated by PXRD and TGA (SI, Figures S12 and S13). Motivated by these highlighted features, MOF-590 was employed as a reusable catalyst in the one-pot oxidative carboxylation of styrene and CO₂ forming styrene carbonate.

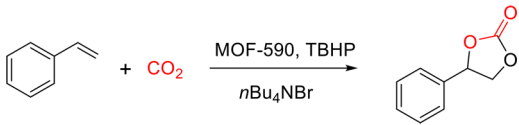
According to crystal structure of MOF-590, the interaction of the substrate molecules is assumed to originate on the external surface of MOF-590. Consequently, FT-IR studies were performed on the samples consisting of the activated MOF-590 in contact with TBHP (MOF-590@TBHP) and styrene oxide (MOF-590@SO) in order to confirm the absorption of the substrates onto this material despite its nonporous nature (SI, Section S8, Figures S29 and S30). Accordingly, the emergence of peaks at 844 and 1028 cm^{-1} in the IR spectra of MOF-590@TBHP and MOF-590@SO, respectively, was observed owing to the characteristic peaks of peroxide O–O stretching and alkoxide C–O–C stretching, respectively.^{25,55} The active Nd clusters of MOF-590 can serve as Lewis acid catalytic sites to react with TBHP and activate the epoxy ring through the oxygen atoms. These results validate the ability of MOF-590 to adsorb organic substrates onto the external surface.

In order to obtain an optimized reaction condition, we first used MOF-590 as a model platform to investigate the impact of catalyst amount, with the use of styrene (3.9 mmol), a co-

catalyst $n\text{Bu}_4\text{NBr}$ (8 mol %), anhydrous TBHP (1.9 equiv), and solvent-free at 80 °C under atmosphere pressure of CO_2 for 12 h. Accordingly, the reaction using 0.09 mol % catalyst proceeded to 88% conversion of styrene and 86% yield of styrene carbonate.

The conversion, selectivity, and yield of the oxidative carboxylation of styrene and CO_2 increased to 96, 95, and 91%, respectively, upon increasing the amount of catalyst to 0.18 mol %. However, a further increase to 0.27 mol % MOF-590 was found to be ineffective, resulting in lower conversion of styrene (90%) and yield of carbonate product (63%) (Table 3, SI, Figures S34–S35). It was noted that the generation of

Table 3. Optimization of MOF-590 Amount for One-Pot Oxidative Carboxylation of Styrene and CO_2 ^a



no.	MOF-590 (mol %)	con. (%) ^b	sel. (%) ^b	yield (%) ^b	
				SC	SO
1	0.09	88	97	86	3
2	0.18	96	95	91	0
3	0.27	90	70	63	0
4	No-MOF	92	41	38	7

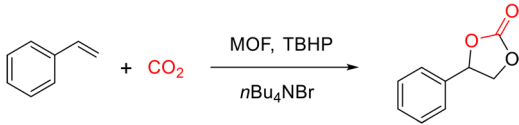
^aReaction conditions: styrene (3.9 mmol), TBHP in decane (7.4 mmol), $n\text{Bu}_4\text{NBr}$ (8 mol %), CO_2 (balloon pressure), 80 °C, 12 h.

^bThe catalytic conversion (con.) of styrene, selectivity (sel.) of styrene carbonate, and yield of products were quantified by GC-FID with the use of biphenyl as the internal standard. SC = styrene carbonate; SO = styrene oxide.

styrene oxide was observed to be 0 in the presence of 0.18 and 0.27 mol % catalyst. In a control experiment, we found that only 38% yield of cyclic carbonate product was obtained when reactions were carried out in the absence of MOF catalyst (Table 3, entry 4). *tert*-Butanol (*t*-BuOH) was permanently observed as a byproduct of the oxidation transformation. To emphasize the reproducibility of catalytic results, all catalytic reactions were conducted at least three times, and the results obtained in standard deviations of ± 2 , ± 2 , and ± 3 % for the conversion, selectivity, and yield of the products, respectively.

With the optimized condition, the catalytic activities of all three compounds MOF-590 to -592 were examined for the one-pot oxidative carboxylation of CO_2 with styrene to obtain styrene carbonate. MOF-590 demonstrated the best performance in the Ln-MOF series (Table 4) reaching 93% conversion, a selectivity of 94%, and 87% yield after 10 h at 80 °C under 1 atm of CO_2 . A small amount of styrene oxide still remained (ca. 3%) after 10 h (Table 4, entry 1), but it was unobserved after 12 h, indicating a completeness of oxidation of styrene (Table 3, entry 2). As such, MOF-590 afforded the highest selectivity and yield of styrene carbonate (95 and 91%, respectively) after 12 h. Interestingly, MOF-590 promoted reasonable catalysis for the synthesis of styrene carbonate with the use of aqueous TBHP, yielding high conversion and good yield of 97 and 84%, respectively (Table 4, entry 2, SI, Figure S36). Otherwise, MOF-591 and -592 exhibited high conversion of styrene (95 and 98%, respectively) with reasonable yields of styrene carbonate (80–81%) (Table 4, entries 3 and 4).

Table 4. Optimization of Reaction Conditions for One-Pot Oxidative Carboxylation of Styrene and CO_2 Catalyzed by MOF-590, -591, and -592^a

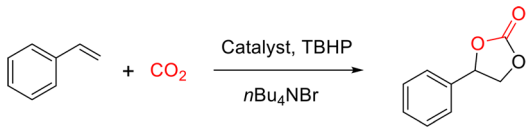


no.	MOF	con. (%) ^c	sel. (%) ^c	yield (%) ^c	
				SC	SO
1	MOF-590	93	94	87	3
2 ^b	MOF-590	97	87	84	8
3	MOF-591	95	85	81	3
4	MOF-592	98	82	80	5

^aReaction conditions: styrene (3.9 mmol), MOF (0.18 mol %, based on molecular weight), TBHP in decane (7.4 mmol), $n\text{Bu}_4\text{NBr}$ (8 mol %), CO_2 (balloon pressure), 80 °C, 10 h. ^bTBHP in H_2O . ^cThe catalytic conversion (con.) of styrene, selectivity (sel.) of styrene carbonate, and yield of products were determined by GC-FID analysis using biphenyl as the internal standard. SC = styrene carbonate; SO = styrene oxide.

To compare the catalytic efficiency of these MOF catalysts, we performed the typical oxidative carboxylation reaction using homogeneous catalysts and Lewis acidic-MOF materials (Table 5). Accordingly, MOF-590 was shown to be the best catalyst among the evaluated catalytic platforms. In general, the homogeneous metal salts, $\text{Nd}(\text{NO}_3)_3 \cdot 6\text{H}_2\text{O}$, $\text{Eu}(\text{NO}_3)_3 \cdot 5\text{H}_2\text{O}$, and $\text{Tb}(\text{NO}_3)_3 \cdot x\text{H}_2\text{O}$ exhibited poorer performances than those of MOF-590 (Table 5, entries 1–3). Low selectivities (55, 30, 52%) and yields (48, 27, 47%) of styrene carbonate formation were found with the homogeneous Nd, Eu, and Tb salt catalysts, respectively, even though high conversions (88, 92, 90%, respectively) were initially observed. Additionally, the reaction using just the $\text{H}_4\text{BIPA-TC}$ linker afforded only 38% yield of styrene carbonate with a moderate conversion of styrene (66%, Table 5, entry 4). Interestingly, a reaction catalyzed by a mixture of $\text{Nd}(\text{NO}_3)_3 \cdot 6\text{H}_2\text{O}$ and $\text{H}_4\text{BIPA-TC}$ linker proceeded a high conversion of styrene (91%), but only 41% yield of styrene carbonate form under the model reaction (Table 5, entry 5). These evidences support the high catalytic activity of Ln sites and the cooperative effect between the Ln clusters and the naphthalene diimide based linker within MOF-590, -591, and -592.

Similarly, the MOF-based catalysts Al-MIL-53,⁴⁴ UiO-67-bpydc,²² and ZIF-8⁴⁵ exhibited low yields of 38, 39, and 22%, respectively, under identical condition (Table 5, entries 9–11). HKUST-1⁴⁶ showed no catalytic activity for the carbonate synthesis with 99% conversion of styrene to benzaldehyde and 2-hydroxy-2-phenylethyl benzoate, and only a trace amount of both styrene oxide and styrene carbonate were detected (Table 5, entry 12). Similarly, MOF-177⁴⁷ and Mg-MOF-74²² promoted the one-pot synthesis of styrene carbonate from styrene and CO_2 with moderate yields of 53 and 50%, respectively (Table 5, entries 13 and 14). By comparing these results, it is evident that high surface area and high CO_2 total uptake at room temperature are not the most decisive variables for the catalytic activity in the one-pot oxidative carboxylation. This is evidenced by the exceptional yield and the even more exceptional selectivity achieved by nonporous MOF-590 as opposed to the other representative MOFs with high porosity, such as MOF-177, Mg-MOF-74, MOF-591, and MOF-592. In particular, reaction using other nonporous Nd-based MOF,

Table 5. Comparison of Catalysts for One-Pot Oxidative Carboxylation of Styrene^a


no.	type	catalyst	con. (%) ^c	sel. (%) ^c	yield (%) ^c	
					SC	SO
1	Hom.	Nd(NO ₃) ₃ ·6H ₂ O	88	55	48	15
2		Eu(NO ₃) ₃ ·5H ₂ O	92	30	27	13
3		Tb(NO ₃) ₃ ·xH ₂ O	90	52	47	15
4		H ₄ BIPA-TC	66	57	38	10
5		H ₄ BIPA-TC + Nd(NO ₃) ₃ ·6H ₂ O	91	45	41	12
6	MOF	MOF-590	93	94	87	3
7		MOF-591	95	85	81	3
8		MOF-592	98	82	80	5
9		Al-MIL-53	77	49	38	15
10 ^b		UiO-67	62	63	39	20
11		ZIF-8	67	33	22	12
12		HKUST-1	99 ^d	0	0	0
13		MOF-177	97	54	53	12
14 ^b		Mg-MOF-74	82	61	50	14
15 ^b		Nd-BDC	98	52	51	0

^aReaction conditions: styrene (3.9 mmol), MOF (0.18 mol %, based on molecular weight), TBHP in decane (7.4 mmol), *n*Bu₄NBr (8 mol %), CO₂ (balloon pressure), 80 °C, 10 h. ^bMolecular weight calculated from Zr₆O₄(OH)₄(C₁₂N₂O₄H₆)₆, Mg₂(C₈O₆H₂)(H₂O)₂, and Nd₂(C₈O₄H₄)₃(DMF)₃(H₂O) for UiO-67-bpydc, Mg-MOF-74, and Nd-BDC, respectively. Hom. = homogeneous; SC = styrene carbonate; and SO = styrene oxide. ^cThe catalytic conversion (con.) of styrene, selectivity (sel.) of styrene carbonate, and yield of products were quantified by GC-FID analysis and the use of biphenyl as the internal standard. ^dBenzaldehyde and 2-hydroxy-2-phenylethyl benzoate were observed as main products.

Nd-BDC,⁴⁸ provided only 51% yield of styrene carbonate (Table 5, entry 15). This result confirms the outstanding structure–function of MOF-590 framework, the combinations of Nd clusters and naphthalene diimide-based linker, for the catalysis oxidative carboxylation reaction of styrene and CO₂.

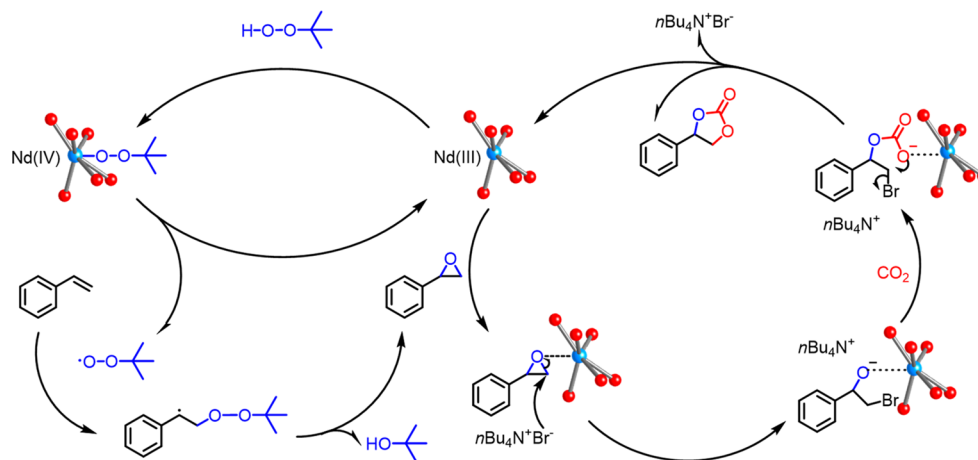
To confirm the heterogeneous nature of MOF-590, we performed a leaching assessment for the model reaction to prove that the catalytic activity did not promote from any Nd³⁺ ions leaching from the MOF-590 structure. After the catalytic reactions were carried out for 2 and 6 h, MOF-590 catalyst was removed by centrifugation, and the filtrated reactions were allowed to continue for 12 h. As expected, there was no significant increase of the yield of styrene carbonate in the 6 h filtrate reaction (rate of increasing yield of 1%), nor the 2 h filtrate (6% rate of increasing yield). We notice that this virtual quenching of the reaction after the solid catalyst removal is different from the results of the blank experiment conducted without MOF, where there is a higher increase of the yield (23% in the initial 6 h, and 7.4% in the final 6 h, Figure S37). However, it must be considered that after solid filtration, the reaction medium is expected to be different in each case, due to inevitable withdrawing of unknown amounts of TBHP, styrene oxide, and *n*Bu₄NBr absorbed to the surface of MOF-590, and thus the two systems are not directly comparable. Nonetheless, the hot filtration experiment demonstrates the heterogeneous nature of the system catalyzed by MOF-590. Furthermore, the filtrates were also analyzed with inductively coupled plasma mass spectrometry (ICP-MS), and the concentration of Nd³⁺ was found to be <3 ppm, indicative of no considerable Nd³⁺ leaching in the reaction solutions. To assess the reusability of MOF-590 catalyst, recycling studies were conducted under the optimized condition. Remarkably, MOF-590 was recovered and reused up to five times without a significant decrease in catalytic activity, demonstrated by the reasonable average values of conversion (88%), selectivity (90%), and yield (79%) of styrene carbonate (SI, Section S9, Figure S38). The structural crystalline of the recycled MOF-590 catalyst was proven by PXRD (SI, Section S10, Figure S39). In addition, the integrity and particle morphology of MOF-590 were retained after several catalytic reactions, as indicated by FT-IR analyses (SI, Figure S40) and SEM images (SI, Figure S41).

The direct synthesis of styrene carbonate from styrene and CO₂ can be described as an oxidative carboxylation process that combines two consecutive reactions: (i) the epoxidation of styrene and (ii) the following cycloaddition of CO₂ to styrene oxide. To gain more information on the role of the catalyst, both reactions, epoxidation of styrene (first step) and

Table 6. Study of the Influence of Reaction Variables on the Two Reactions Part of the Oxidative Carboxylation of Styrene and CO₂^a

no.	sub.	pro.	MOF-590	<i>n</i> Bu ₄ NBr	TBHP	CO ₂	con. (%) ^c	sel. (%) ^c	yield (%) ^c	
									SC	SO
1	ST	SO	+	0	+	0	42	—	—	22
2	ST	SO	0	0	+	0	16	—	—	15
3	ST	SO	+	+	+	0	68	—	—	45
4	ST	SO	0	+	+	0	47	—	—	28
5 ^b	SO	SC	+	+	+	+	94	82	77	—
6 ^b	SO	SC	0	+	+	+	90	71	64	—
7 ^b	SO	SC	+	+	0	+	87	99	86	—
8 ^b	SO	SC	0	+	0	+	32	90	29	—

^aReaction conditions: styrene (3.9 mmol), MOF (0.18 mol %), TBHP in decane (7.4 mmol), *n*Bu₄NBr (8 mol %), CO₂ (balloon pressure), 80 °C, 10 h. ^bReaction conditions: styrene oxide (3.9 mmol), MOF (0.18 mol %), TBHP in decane (7.4 mmol), *n*Bu₄NBr (8 mol %), CO₂ (balloon pressure), 80 °C, 10 h. ^cThe catalytic conversion (con.) of styrene, selectivity (sel.) of styrene carbonate, and yield were calculated by GC-FID analysis using biphenyl as the internal standard. sub. = substrate; pro. = product; ST = styrene; SC = styrene carbonate; SO = styrene oxide; (+) = presence, (0) = none.

Scheme 1. Proposed Mechanism for the Oxidative Carboxylation of Styrene and CO₂ Catalyzed by MOF-590

cycloaddition of CO₂ to styrene oxide (second step), were independently carried out (Table 6). Consequently, the epoxidation experiments for the first step were carried out under the same conditions without the use of CO₂ (Table 6, entries 1–4). Accordingly, in the presence of MOF-590 as catalyst, the reaction proceeded with a conversion/yield of 42/22%, while in absence of catalyst, a conversion/yield of 8/15% was achieved (Table 6, entries 1 and 2). *n*Bu₄NBr was also found to catalyze the reaction, reaching a conversion/yield of 47/28%, and, when combining both MOF-590 and *n*Bu₄NBr, the best performance was observed with a conversion/yield of 68/45% (Table 6, entries 3 and 4).

As expected, minor quantities of benzaldehyde and 2-hydroxy-2-phenylethyl benzoate were detected as side products of the one-pot oxidative carboxylation reaction (SI, Section S4, Figure S42). This observation was consistent with previous reports, which demonstrated the catalytic activity of *n*Bu₄NBr in the oxidative carboxylation through the bromohydrin species in situ assumption.^{28,49,50}

With our results, the important role of *n*Bu₄NBr in both the epoxidation of styrene and the cycloaddition of CO₂ to styrene oxide is evidenced, which also proceeds with good conversion and moderate yield (90 and 64% respectively) in absence of MOF and presence of TBHP (Table 6, entry 6). However, in the absence of TBHP and MOF-590, only 32% conversion and 29% yield were observed. MOF-590 exhibited an exceptional catalytic activity toward the cycloaddition of CO₂ to styrene oxide, with conversion of 87%, selectivity of 99%, and yield of 86% in the formation of styrene carbonate in absence of TBHP and *n*Bu₄NBr (Table 6, entry 7). The selectivity to the formation of styrene carbonate was slightly diminished through the addition of TBHP (82%, Table 6, entry 5).

The combination of both MOF-590 and *n*Bu₄NBr results in a highly efficient catalytic system for the addition of CO₂ to styrene oxide, reaching 94% conversion and 77% yield of styrene carbonate in the presence of TBHP (Table 6, entry 5) and 87% conversion and 86% yield of styrene carbonate in absence of TBHP (Table 6, entry 7). It is suggested that the Lewis and/or Brønsted acid sites derived from Nd clusters of MOF-590 work together with the base *n*Bu₄NBr co-catalyst to complete the activation of the epoxy ring for the cycloaddition of CO₂ and styrene oxide. On the other hand, with the use of aqueous TBHP (Table 4, entry 3), the conversion of styrene and the amounts of styrene oxide, benzaldehyde, and 2-hydroxy-2-phenylethyl benzoate were also found to slightly

increase as compared to those found with the use of anhydrous TBHP, indicating that the impact of water on the one-pot oxidative carboxylation catalyzed by MOF-590 is minimal.

An epoxidation catalyzed by metal-based catalyst has been reported to proceed through a radical pathway.^{51–54} In order to demonstrate if radicals were involved in such reactions, a radical scavenger, 2,2,6,6-tetramethylpiperidine 1-oxyl (TEMPO, 1 equiv to mole of TBHP), was added separately into the model experiments of the epoxidation reaction and the oxidative carboxylation reaction after 2 h (SI, Section S11, Figure S43). Consequently, the reactions were continued under the same condition and monitored for 10 h. It was observed that the yield of styrene oxide (14%) obtained from epoxidation reaction was lower than that of typical epoxidation reactions (45%, Table 6, entry 3). Notably, upon addition of the radical scavenger, the oxidative carboxylation reaction ended immediately with 17% yield of styrene carbonate after 10 h (SI, Section S11, Figure S43). Therefore, we suggest that the overall mechanism of oxidative carboxylation indeed proceeds mainly via radical process.

Plausible Reaction Mechanism. Based on our observations and previous literature, the mechanism of the oxidative carboxylation of styrene and CO₂ should consist of the mechanism of the epoxidation catalyzed by MOF-590/*n*Bu₄NBr-TBHP and the mechanism of the subsequent cycloaddition catalyzed by MOF-590/*n*Bu₄NBr. Accordingly, in light of the catalytic contribution of MOF-590 catalyst, the radical pathway depicted in Scheme 1 takes place between Nd³⁺ clusters of MOF-590 and TBHP to form Nd⁴⁺-peroxy species.^{53,54,56–58} The Nd⁴⁺-peroxy species then releases a *t*-butoxy radical and regenerates MOF-590. Consequently, a reaction between *t*-butoxy radical and styrene produces a *t*-butoxperoxy intermediate, which further undergoes migration of oxygen to yield the styrene oxide product, along with *t*-BuOH as byproduct. An involvement of oxygen with *t*-butoxperoxy intermediate could result in benzaldehyde as the side product.

Subsequently, in the cycloaddition of CO₂ to styrene oxide reaction, the O atom of styrene oxide is first activated through an involved coordination of the Nd unit. The epoxide coordination molecule is accordingly attacked by Br[−] acting as nucleophile derived from the co-catalyst *n*Bu₄NBr, leading to form a metal-coordinated bromoalkoxide. The CO₂ molecules then insert into the Nd–O bonds, forming metal-carbonate intermediates. Finally, a ring-closing step of metal–

carbonate intermediate takes place, in which a styrene carbonate is formed, and, simultaneously, the MOF-590 catalyst and $n\text{Bu}_4\text{NBr}$ co-catalyst are regenerated (Scheme 1).

SUMMARY

In conclusion, the synthesis and full characterization of a novel series of lanthanide-based MOFs constructed from a benzoimidephenanthroline tetracarboxylic acid linker were demonstrated. MOF-591 and MOF-592 showed moderate CO_2 uptake capacities at 800 Torr and 298 K (36 and 42 $\text{cm}^3 \text{g}^{-1}$, respectively) with corresponding zero coverage isosteric heats of adsorption being 23 and 22 kJ mol^{-1} , respectively. To ensure the selective CO_2 adsorption property, breakthrough measurements were employed on MOF-592 with a binary gas mixture containing CO_2 and N_2 . As expected, MOF-592 was proven as a promising adsorbent for the CO_2 separation over N_2 (1.2 wt % CO_2 capacity). The effective CO_2 separation by MOF-592 was successfully demonstrated in three consecutive cycles of dynamic measurement with simple N_2 flow for regeneration. Otherwise, all of the new Ln-MOFs revealed promising catalytic activity for the heterogeneous one-pot oxidative carboxylation of styrene and CO_2 affording styrene carbonate. These materials exhibited excellent conversion, selectivity, and yield of styrene carbonate under soft reaction conditions, in absence of solvent, 1 atm pressure of CO_2 , and 80 °C for 10 h, without the need of preliminary isolation of styrene oxide. Remarkably, MOF-590 was found to be an excellent recyclable catalyst with the use of anhydrous and aqueous TBHP oxidant in the oxidative carboxylation reaction.

ASSOCIATED CONTENT

Supporting Information

The Supporting Information is available free of charge on the ACS Publications website at DOI: 10.1021/acs.inorgchem.8b02293.

Full details for linker and MOF synthesis and characterizations (PXRD, TGA curves, FT-IR, and gas adsorption), crystallographic data, and catalytic reaction details (PDF)

Accession Codes

CCDC 1831029–1831031 contain the supplementary crystallographic data for this paper. These data can be obtained free of charge via www.ccdc.cam.ac.uk/data_request/cif, or by emailing data_request@ccdc.cam.ac.uk, or by contacting The Cambridge Crystallographic Data Centre, 12 Union Road, Cambridge CB2 1EZ, UK; fax: +44 1223 336033.

AUTHOR INFORMATION

Corresponding Authors

*E-mail: gandara@icmm.csic.es.

*E-mail: ntkphuong@inomar.edu.vn.

ORCID

Huong T. D. Nguyen: 0000-0002-7965-9742

Felipe Gándara: 0000-0002-1671-6260

Phuong T. K. Nguyen: 0000-0002-9149-2279

Funding

This work was financially supported by Vietnam National University Ho Chi Minh City (VNU-HCM) under grant C2018-50-03. F.G. acknowledges Spanish Ministry of Economy and Competitiveness for funding through the “Ramón y Cajal” program and grant CTQ2017–87262-R.

Notes

The authors declare no competing financial interest.

ACKNOWLEDGMENTS

We are grateful to Prof. O. M. Yaghi (UC Berkeley), Mr. Kyle E. Cordova (UC Berkeley), and the Berkeley Global Science Institute for continuous support of research activities. We wish to thank Dr. H. Furukawa (UC Berkeley), Prof. Jaheon Kim (Soongsil University), and Dr. H. T. C. Ho for scientific inspirations and valuable discussions. We are indebted to Prof. M. O’Keeffe (Arizona State University) for his useful discussion on topological analysis.

REFERENCES

- (1) Furukawa, H.; Cordova, K. E.; O’Keeffe, M.; Yaghi, O. M. The Chemistry and Applications of Metal–Organic Frameworks. *Science* **2013**, *341*, 1230444.
- (2) Li, M.; Li, D.; O’Keeffe, M.; Yaghi, O. M. Topological Analysis of Metal–Organic Frameworks with Polytopic Linkers and/or Multiple Building Units and the Minimal Transitivity Principle. *Chem. Rev.* **2014**, *114*, 1343–1370.
- (3) Müller-Buschbaum, K., Group 3 Elements and Lanthanide Metals. In *The Chemistry of Metal–Organic Frameworks*; Wiley-VCH Verlag GmbH & Co. KGaA: Weinheim, Germany, 2016; Chapter 9, pp 231–270.
- (4) Noh, H.; Cui, Y.; Peters, A. W.; Pahls, D. R.; Ortuño, M. A.; Vermeulen, N. A.; Cramer, C. J.; Gagliardi, L.; Hupp, J. T.; Farha, O. K. An Exceptionally Stable Metal–Organic Framework Supported Molybdenum(VI) Oxide Catalyst for Cyclohexene Epoxidation. *J. Am. Chem. Soc.* **2016**, *138*, 14720–14726.
- (5) Beyzavi, M. H.; Klet, R. C.; Tussupbayev, S.; Borycz, J.; Vermeulen, N. A.; Cramer, C. J.; Stoddart, J. F.; Hupp, J. T.; Farha, O. K. A Hafnium-Based Metal–Organic Framework as an Efficient and Multifunctional Catalyst for Facile CO_2 Fixation and Regioselective and Enantioselective Epoxide Activation. *J. Am. Chem. Soc.* **2014**, *136*, 15861–15864.
- (6) Ma, J.-x.; Guo, J.; Wang, H.; Li, B.; Yang, T.; Chen, B. Microporous Lanthanide Metal–Organic Framework Constructed from Lanthanide Metalloligand for Selective Separation of $\text{C}_2\text{H}_2/\text{CO}_2$ and $\text{C}_2\text{H}_2/\text{CH}_4$ at Room Temperature. *Inorg. Chem.* **2017**, *56*, 7145–7150.
- (7) He, Y.; Furukawa, H.; Wu, C.; O’Keeffe, M.; Krishna, R.; Chen, B. Low-Energy Regeneration and High Productivity in a Lanthanide-Hexacarboxylate Framework for High-Pressure CO_2 - CH_4 - H_2 Separation. *Chem. Commun.* **2013**, *49*, 6773–6775.
- (8) Lee, W. R.; Ryu, D. W.; Lee, J. W.; Yoon, J. H.; Koh, E. K.; Hong, C. S. Microporous Lanthanide–Organic Frameworks with Open Metal Sites: Unexpected Sorption Propensity and Multifunctional Properties. *Inorg. Chem.* **2010**, *49*, 4723–4725.
- (9) Luo, J.; Xu, H.; Liu, Y.; Zhao, Y.; Daemen, L. L.; Brown, C.; Timofeeva, T. V.; Ma, S.; Zhou, H.-C. Hydrogen Adsorption in a Highly Stable Porous Rare-Earth Metal–Organic Framework: Sorption Properties and Neutron Diffraction Studies. *J. Am. Chem. Soc.* **2008**, *130*, 9626–9627.
- (10) D’Vries, R. F.; Iglesias, M.; Snejko, N.; Gutiérrez-Puebla, E.; Monge, M. A. Lanthanide Metal–Organic Frameworks: Searching for Efficient Solvent-Free Catalysts. *Inorg. Chem.* **2012**, *51*, 11349–11355.
- (11) Dang, D.; Bai, Y.; He, C.; Wang, J.; Duan, C.; Niu, J. Structural and Catalytic Performance of a Polyoxometalate-Based Metal–Organic Framework Having a Lanthanide Nanocage as a Secondary Building Block. *Inorg. Chem.* **2010**, *49*, 1280–1282.
- (12) Zhu, Y.; Zhu, M.; Xia, L.; Wu, Y.; Hua, H.; Xie, J. Lanthanide Metal–Organic Frameworks with Six-Coordinated Ln(III) Ions and Free Functional Organic Sites for Adsorptions and Extensive Catalytic Activities. *Sci. Rep.* **2016**, *6*, 29728.

- (13) Liu, Y.; Mo, K.; Cui, Y. Porous and Robust Lanthanide Metal-Organoboron Frameworks as Water Tolerant Lewis Acid Catalysts. *Inorg. Chem.* **2013**, *52*, 10286–10291.
- (14) Trickett, C. A.; Helal, A.; Al-Maythaly, B. A.; Yamani, Z. H.; Cordova, K. E.; Yaghi, O. M. The Chemistry of Metal–Organic Frameworks for CO₂ Capture, Regeneration and Conversion. *Nat. Rev. Mater.* **2017**, *2*, 17045.
- (15) Yuan, Z.; Eden, M. R.; Gani, R. Toward the Development and Deployment of Large-Scale Carbon Dioxide Capture and Conversion Processes. *Ind. Eng. Chem. Res.* **2016**, *55*, 3383–3419.
- (16) Sumida, K.; Rogow, D. L.; Mason, J. A.; McDonald, T. M.; Bloch, E. D.; Herm, Z. R.; Bae, T. H.; Long, J. R. Carbon Dioxide Capture in Metal–Organic Frameworks. *Chem. Rev.* **2012**, *112*, 724–781.
- (17) Fracaroli, A. M.; Furukawa, H.; Suzuki, M.; Dodd, M.; Okajima, S.; Gándara, F.; Reimer, J. A.; Yaghi, O. M. Metal–Organic Frameworks with Precisely Designed Interior for Carbon Dioxide Capture in the Presence of Water. *J. Am. Chem. Soc.* **2014**, *136*, 8863–8866.
- (18) Nguyen, P. T. K.; Nguyen, H. T. D.; Pham, H. Q.; Kim, J.; Cordova, K. E.; Furukawa, H. Synthesis and Selective CO₂ Capture Properties of a Series of Hexatopic Linker-Based Metal–Organic Frameworks. *Inorg. Chem.* **2015**, *54*, 10065–10072.
- (19) Nguyen, N. T. T.; Lo, T. N. H.; Kim, J.; Nguyen, H. T. D.; Le, T. B.; Cordova, K. E.; Furukawa, H. Mixed-Metal Zeolitic Imidazolate Frameworks and Their Selective Capture of Wet Carbon Dioxide over Methane. *Inorg. Chem.* **2016**, *55*, 6201–6207.
- (20) Nguyen, N. T. T.; Furukawa, H.; Gándara, F.; Nguyen, H. T.; Cordova, K. E.; Yaghi, O. M. Selective Capture of Carbon Dioxide under Humid Conditions by Hydrophobic Chabazite-Type Zeolitic Imidazolate Frameworks. *Angew. Chem., Int. Ed.* **2014**, *53*, 10645–10648.
- (21) Liu, Q.; Wu, L.; Jackstell, R.; Beller, M. Using Carbon Dioxide as a Building Block in Organic Synthesis. *Nat. Commun.* **2015**, *6*, 5933.
- (22) Nguyen, P. T. K.; Nguyen, H. T. D.; Nguyen, H. N.; Trickett, C. A.; Ton, Q. T.; Gutiérrez-Puebla, E.; Monge, M. A.; Cordova, K. E.; Gándara, F. New Metal–Organic Frameworks for Chemical Fixation of CO₂. *ACS Appl. Mater. Interfaces* **2018**, *10*, 733–744.
- (23) Zhu, J.; Usov, P. M.; Xu, W.; Celis-Salazar, P. J.; Lin, S.; Kessinger, M. C.; Landaverde-Alvarado, C.; Cai, M.; May, A. M.; Slebodnick, C.; Zhu, D.; Senanayake, S. D.; Morris, A. J. A New Class of Metal–Cyclam-Based Zirconium Metal–Organic Frameworks for CO₂ Adsorption and Chemical Fixation. *J. Am. Chem. Soc.* **2018**, *140*, 993–1003.
- (24) Xu, H.; Zhai, B.; Cao, C.-S.; Zhao, B. A Bifunctional Europium–Organic Framework with Chemical Fixation of CO₂ and Luminescent Detection of Al³⁺. *Inorg. Chem.* **2016**, *55*, 9671–9676.
- (25) Guo, X.; Zhou, Z.; Chen, C.; Bai, J.; He, C.; Duan, C. New Rht-Type Metal–Organic Frameworks Decorated with Acylamide Groups for Efficient Carbon Dioxide Capture and Chemical Fixation from Raw Power Plant Flue Gas. *ACS Appl. Mater. Interfaces* **2016**, *8*, 31746–31756.
- (26) Dong, J.; Xu, H.; Hou, S.-L.; Wu, Z.-L.; Zhao, B. Metal–Organic Frameworks with Tb₄ Clusters as Nodes: Luminescent Detection of Chromium(VI) and Chemical Fixation of CO₂. *Inorg. Chem.* **2017**, *56*, 6244–6250.
- (27) Liang, J.; Chen, R.-P.; Wang, X.-Y.; Liu, T.-T.; Wang, X.-S.; Huang, Y.-B.; Cao, R. Postsynthetic Ionization of an Imidazole-Containing Metal–Organic Framework for the Cycloaddition of Carbon Dioxide and Epoxides. *Chem. Sci.* **2017**, *8*, 1570–1575.
- (28) Sun, J.; Fujita, S.-i.; Bhanage, B. M.; Arai, M. One-Pot Synthesis of Styrene Carbonate from Styrene in Tetrabutylammonium Bromide. *Catal. Today* **2004**, *93–95*, 383–388.
- (29) Chen, F.; Dong, T.; Xu, T.; Li, X.; Hu, C. Direct Synthesis of Cyclic Carbonates from Olefins and CO₂ Catalyzed by a MoO₂(acac)₂-Quaternary Ammonium Salt System. *Green Chem.* **2011**, *13*, 2518–2524.
- (30) Maksimchuk, N. V.; Ivanchikova, I. D.; Ayupov, A. B.; Kholdeeva, O. A. One-Step Solvent-Free Synthesis of Cyclic Carbonates by Oxidative Carboxylation of Styrenes over a Recyclable Ti-Containing Catalyst. *Appl. Catal., B* **2016**, *181*, 363–370.
- (31) Han, Q.; Qi, B.; Ren, W.; He, C.; Niu, J.; Duan, C. Polyoxometalate-Based Homochiral Metal–Organic Frameworks for Tandem Asymmetric Transformation of Cyclic Carbonates from Olefins. *Nat. Commun.* **2015**, *6*, 10007.
- (32) Han, L.; Qin, L.; Xu, L.; Zhou, Y.; Sun, J.; Zou, X. A Novel Photochromic Calcium-Based Metal–Organic Framework Derived from a Naphthalene Diimide Chromophore. *Chem. Commun.* **2013**, *49*, 406–408.
- (33) Al Kobaisi, M.; Bhosale, S. V.; Latham, K.; Raynor, A. M.; Bhosale, S. V. Functional Naphthalene Diimides: Synthesis, Properties, and Applications. *Chem. Rev.* **2016**, *116*, 11685–11796.
- (34) All MOF numbers in this paper were assigned through Berkeley Global Science Institute submission request, <http://globalscience.berkeley.edu/netcentre> (accessed May 22, 2018).
- (35) APEX3 v 2015.5–2; Bruker AXS Inc.: Madison, Wisconsin, 2015.
- (36) SAINT v 8.37A; Bruker AXS Inc.: Madison, Wisconsin, 2015.
- (37) SADABS 2016/2; Bruker AXS Inc.: Madison, Wisconsin, 2016.
- (38) Sheldrick, G. A Short History of Shelx. *Acta Crystallogr., Sect. A: Found. Crystallogr.* **2008**, *64*, 112–122.
- (39) Dolomanov, O. V.; Bourhis, L. J.; Gildea, R. J.; Howard, J. A. K.; Puschmann, H. Olex2: A Complete Structure Solution, Refinement and Analysis Program. *J. Appl. Crystallogr.* **2009**, *42*, 339–341.
- (40) Blatov, V. A.; Shevchenko, A. P.; Proserpio, D. M. Applied Topological Analysis of Crystal Structures with the Program Package Topospro. *Cryst. Growth Des.* **2014**, *14*, 3576–3586.
- (41) Li, M.; Li, D.; O’Keeffe, M.; Yaghi, O. M. Topological Analysis of Metal–Organic Frameworks with Polytopic Linkers and/or Multiple Building Units and the Minimal Transitivity Principle. *Chem. Rev.* **2014**, *114*, 1343–1370.
- (42) Spek, A. L. Structure validation in chemical crystallography. *Acta Crystallogr., Sect. D: Biol. Crystallogr.* **2009**, *65*, 148–155.
- (43) Frisch, M. J.; Trucks, G. W.; Schlegel, H. B.; Scuseria, G. E.; Robb, M. A.; Cheeseman, J. R.; Scalmani, G.; Barone, V.; Mennucci, B.; Petersson, G. A.; Nakatsuji, H.; Caricato, M.; Li, X.; Hratchian, H. P.; Izmaylov, A. F.; Bloino, J.; Zheng, G.; Sonnenberg, J. L.; Hada, M.; Ehara, M.; Toyota, K.; Fukuda, R.; Hasegawa, J.; Ishida, M.; Nakajima, T.; Honda, Y.; Kitao, O.; Nakai, H.; Vreven, T.; Montgomery, J. A., Jr.; Peralta, J. E.; Ogliaro, F.; Bearpark, M.; Heyd, J. J.; Brothers, E.; Kudin, K. N.; Staroverov, V. N.; Kobayashi, R.; Normand, J.; Raghavachari, K.; Rendell, A.; Burant, J. C.; Iyengar, S. S.; Tomasi, J.; Cossi, M.; Rega, N.; Millam, J. M.; Klene, M.; Knox, J. E.; Cross, J. B.; Bakken, V.; Adamo, C.; Jaramillo, J.; Gomperts, R.; Stratmann, R. E.; Yazyev, O.; Austin, A. J.; Cammi, R.; Pomelli, C.; Ochterski, J. W.; Martin, R. L.; Morokuma, K.; Zakrzewski, V. G.; Voth, G. A.; Salvador, P.; Dannenberg, J. J.; Dapprich, S.; Daniels, A. D.; Farkas, O.; Foresman, J. B.; Ortiz, J. V.; Cioslowski, J.; Fox, D. J. *Gaussian09*, revisions D.01 and B.01; Gaussian, Inc.: Wallingford, CT, 2010.
- (44) Biswas, S.; Ahnfeldt, T.; Stock, N. New Functionalized Flexible Al-Mil-53-X (X = -Cl, -Br, -CH₃, -NO, -(OH)₂) Solids: Syntheses, Characterization, Sorption, and Breathing Behavior. *Inorg. Chem.* **2011**, *50*, 9518–9526.
- (45) Wang, B.; Cote, A. P.; Furukawa, H.; O’Keeffe, M.; Yaghi, O. M. Colossal Cages in Zeolitic Imidazolate Frameworks as Selective Carbon Dioxide Reservoirs. *Nature* **2008**, *453*, 207–211.
- (46) Furukawa, H.; Go, Y. B.; Ko, N.; Park, Y. K.; Uribe-Romo, F. J.; Kim, J.; O’Keeffe, M.; Yaghi, O. M. Isorecticular Expansion of Metal–Organic Frameworks with Triangular and Square Building Units and the Lowest Calculated Density for Porous Crystals. *Inorg. Chem.* **2011**, *50*, 9147–9152.
- (47) Furukawa, H.; Miller, M. A.; Yaghi, O. M. Independent Verification of the Saturation Hydrogen Uptake in MOF-177 and Establishment of a Benchmark for Hydrogen Adsorption in Metal–Organic Frameworks. *J. Mater. Chem.* **2007**, *17*, 3197–3204.

- (48) Decadt, R.; Van Hecke, K.; Depla, D.; Leus, K.; Weinberger, D.; Van Driessche, I.; Van Der Voort, P.; Van Deun, R. Synthesis, Crystal Structures, and Luminescence Properties of Carboxylate Based Rare-Earth Coordination Polymers. *Inorg. Chem.* **2012**, *51*, 11623–11634.
- (49) Wang, J.-L.; Wang, J.-Q.; He, L.-N.; Dou, X.-Y.; Wu, F. A CO₂/H₂O₂-Tunable Reaction: Direct Conversion of Styrene into Styrene Carbonate Catalyzed by Sodium Phosphotungstate/*n*-Bu₄NBr. *Green Chem.* **2008**, *10*, 1218–1223.
- (50) Eghbali, N.; Li, C.-J. Conversion of Carbon Dioxide and Olefins into Cyclic Carbonates in Water. *Green Chem.* **2007**, *9*, 213–215.
- (51) Chughtai, A. H.; Ahmad, N.; Younus, H. A.; Laypkov, A.; Verpoort, F. Metal-Organic Frameworks: Versatile Heterogeneous Catalysts for Efficient Catalytic Organic Transformations. *Chem. Soc. Rev.* **2015**, *44*, 6804–6849.
- (52) Dhakshinamoorthy, A.; Asiri, A. M.; Garcia, H. Metal–Organic Frameworks as Catalysts for Oxidation Reactions. *Chem. - Eur. J.* **2016**, *22*, 8012–8024.
- (53) Zhang, J.; Biradar, A. V.; Pramanik, S.; Emge, T. J.; Asefa, T.; Li, J. A New Layered Metal-Organic Framework as a Promising Heterogeneous Catalyst for Olefin Epoxidation Reactions. *Chem. Commun.* **2012**, *48*, 6541–6543.
- (54) Beier, M. J.; Kleist, W.; Wharmby, M. T.; Kissner, R.; Kimmerle, B.; Wright, P. A.; Grunwaldt, J.-D.; Baiker, A. Aerobic Epoxidation of Olefins Catalyzed by the Cobalt-Based Metal–Organic Framework STA-12(Co). *Chem. - Eur. J.* **2012**, *18*, 887–898.
- (55) Vacque, V.; Sombret, B.; Huvenne, J. P.; Legrand, P.; Suc, S. Characterisation of the O-O peroxide bond by vibrational spectroscopy. *Spectrochim. Acta, Part A* **1997**, *53*, 55–66.
- (56) Sheldon, R. A.; Kochi, J. K. Metal Catalysis in Peroxide Reactions. In *Metal-Catalyzed Oxidations of Organic Compounds*; Academic Press: New York, 1981; pp 33–70.
- (57) Lee, J.; Farha, O. K.; Roberts, J.; Scheidt, K. A.; Nguyen, S. T.; Hupp, J. T. Metal-Organic Framework Materials as Catalysts. *Chem. Soc. Rev.* **2009**, *38*, 1450–1459.
- (58) Sebastian, J.; Jinka, K. M.; Jasra, R. V. Effect of Alkali and Alkaline Earth Metal Ions on the Catalytic Epoxidation of Styrene with Molecular Oxygen Using Cobalt(II)-Exchanged Zeolite X. *J. Catal.* **2006**, *244*, 208–218.